

Received August 24, 2021, accepted September 15, 2021, date of publication October 13, 2021, date of current version November 1, 2021.

Digital Object Identifier 10.1109/ACCESS.2021.3119567

Design of a Transverse Flux Permanent Magnet Generator Using a Reluctance Circuit

CRISTHIAN BECKER^{1,2}, (Member, IEEE), MAURICIO VALENCIA FERREIRA DA LUZ¹, AND JEAN VIANEI LEITE¹

¹Electrical and Electronic Engineering Department (EEL), Federal University of Santa Catarina (UFSC), Florianópolis, Santa Catarina 88040-970, Brazil

²Electrical Engineering Department, Faculty of Engineering, University of Santiago of Chile (USACH), Santiago, Región Metropolitana 9170002, Chile

Corresponding author: Cristhian Becker (cristhian.becker@usach.cl)

This work was supported in part by the Coordenação de Aperfeiçoamento de Pessoal Nível Superior—Brazil (CAPES)—Finance Code 001.

ABSTRACT This work presents an analytical methodology to design a permanent magnet transverse flux generator using a reluctance circuit. Unlike other research, it fully indicates the details to design the rotor, stator, and the air gap of the machine, with all its geometry. In the design section, special considerations to determine the outer diameter of the rotor, and the accompanying pole pitch for the U-cores and I-cores are presented. The proposal of an iterative algorithm using a reluctance circuit to calculate the turns of the armature winding and curved trajectories of flux tubes to model the leakage flux that will allow the synchronous inductance calculation also is presented. The proposed methodology allows determining the performance and the lumped parameters of the generator. Furthermore, it provides evidence that with this design it is possible to select the values of standard voltage for electric generators of this topology. The analytical results of the magnetic flux densities, magnetic flux, lumped parameters, electromotive force, terminal voltage, armature current, power factor, and efficiency are compared with 3D finite element method. Analyzing these results, it is possible to verify the good agreement between them.


INDEX TERMS Analytical design, reluctance circuit, 3D finite element method, permanent magnet synchronous machines, synchronous inductance, transverse flux permanent magnet generator.

I. INTRODUCTION

The first work which analyzed the permanent magnet transverse flux generator was issued in 1986. The author, H. Weh refers to it as a special topology with high torque density and high-power density, which are ideal for low-speed direct drives. The focus is on the operation as a motor searching for the production of a high-power density rotor. Additionally, it reviews all the simple topologies, double stator, U-core, I-core, V rotor, and intermediate rotor [1]. The already mentioned work does not specify the design and does not compare the results with the Finite Element Method (FEM). To summarize, it deals with an electric machine with permanent magnets in the rotor, ferromagnetic core (rotor and stator), an armature coil, and a path of excitation magnetic flux which is characteristic of this particular machine.

The denomination of electric machine of transverse-flux topology appears eleven years later [2], [3]. From that moment on, the authors focused on the operation as traction

motors, coinciding with the proposal of possible types of coils for the different types of cores, simple and double (U, C, E, I, and claw pole) trying to obtain high-density torque [4]–[7]. Summarizing, it is studied the transverse topology to operate as a generator, as compared to other radial and axial flux topologies [8] and concluding that the transverse flux topology has lower cost and higher torque density. Continuing with the use of this kind of machine as a generator, in [9] it is compared the transverse flux topology with the traditional radial flux, establishing four differences, and determining as the best topology the transverse flux one in terms of cost, mass, loss of copper, and densities (power, torque, and cost). Then, it is proposed a reluctance circuit with a non-iterative algorithm for design a transverse flux permanent magnet generator, TFPMG of low speed, 5 MW, and 2.7 kV. Afterward, and with the intention of extensive use in wind power generation, light generators are proposed [10]. However, the characteristics of the generator under study are 10 MW, 10 rpm, and 13.89 A. Nothing is said about the terminal voltage, which should remain within the medium voltage for the power and current. Besides, the numeric

The associate editor coordinating the review of this manuscript and approving it for publication was Su Yan .

validation used 2D FEM, which is not appropriate for this kind of topology because of the path of magnetic flux, as this type of machine does not present symmetry axial for a 2D analysis. Additionally, the model proposed considers permanent magnets installed in the twisted U-core of the stator. Moreover, the armature coil is also installed in the same core, making it a complicated construction machine, according to the authors. Both in [9] and [10] the stator topology is twisted U-core.

To avoid deformations in the materials near the air gap region, it is suggested a magnetic flux density of around 1 T [11].

A prototype of a generator coupled to a wave and tidal mechanism was built applying the transverse flux topology, the stator is a C-core with teeth [12]. Although it is also a permanent magnet direct drive generator, in this particular case it was coupled to a marine device with a gearbox to operate in ranges of 5 to 40 rpm, 15 kW, which achieved an efficiency of 88%. Nothing is indicated concerning the voltage of terminals and it is a very particular device as the rotor outer diameter is 6 m, this diameter attends to the required dimensions for the device coupling. It is interesting that during the designing process, reluctance networks to estimate dispersion fluxes were raised and it is used Ampere's law to estimate the magnetic inductions and magnetic flow in specific points.

It is important for this research is the approach of the elliptical cross-section of the stator U-core, it has been estimated that it reduces the use of materials and it improves the distribution of the magnetic-flux density vectors in the core itself [13]. There, what is exposed in [9], selecting one of the topologies the author suggests, modifying the twisted U-core. Those authors worked on a 3 MW, 15 rpm, medium voltage machine.

A transverse-flux typology three-phase generator, of strange geometry, with terminal variables of 3.5 kW, 280 V, and 12 poles [14] is of particular interest as it is a low voltage machine with usual nominal characteristics concerning its low voltage, except for the voltage, but it validates the work concerning the voltage selected by the authors.

Subsequently, a simpler topology is proposed with a U-core machine and with a transverse elliptical section and a flux concentration rotor [15], which the authors denominated fall-back rotor. It is only shown the resulting generator of a very low tension on the terminals, 21.95 V and 954.82 W of power, which is compared to a permanent magnet transverse flux generator, with rectangular cross-section and a rotor without flux concentration. Lumped parameters or losses are not considered. Regarding the latter, the research work [1], [4], [8], [9] does not compare the analytic calculation with FEM. An external fall-back rotor topology, with similar results, is presented by the same authors of [15] in [16].

As for the radial flux topology, there are design books [17]–[19], from where can be taken some suggestions the equations for this paper. In [7], [19], both authors explore

a TFPMG with an outer rotor, where it is indicated that for design the transverse flux topology, it would be enough to focus only on one phase. It is possible because this machine is modular concerning the number of phases, its armature winding are independent, there is no coupling among phases and during its construction, they must be properly assembled to achieve the angular displacement among phases.

The present research proposes an analytical methodology to design a TFPMG of 380 V (220 V per phase), 10 kW, and 300 rpm. The main contribution of this paper is an iterative algorithm that uses a reluctance circuit to calculate the turns of the armature winding and curved trajectories of flux tubes to model the leakage flux. This algorithm allows the calculation of synchronous inductance, magnetic flux densities, and magnetic flux considering the core saturation. Furthermore, with the magnetic flux densities, it is possible to obtain the losses and the efficiency of TFPMG. The algorithm also determines the resistance and the mass of the generator. In addition, geometrically, the external diameter of the rotor is calculated taking into account the geometry of the cross section of the U-core. In this methodology, both the U-core and the I-core are proposed not considering the total extension of the polar pitch. The I-cores are considered to improve the performance of the generator [20].

Besides, it is important to notice that the design tension level, in contrast to the studies already mentioned, is of a standardized level for electric machines [21]. Finally, the analytical results are compared with the 3D-FEM ones.

The application of this TFPMG (380 V, 10 kW and 300 rpm) is for renewable energy, such as energy from sea waves, specifically [22], or small-scale hydroelectric turbines.

Finally, and compared to [1], in table 1 we highlight the novelty in comparison with the other reviewed works.

II. TOPOLOGY AND DESIGN OF THE TFPMG

A. GEOMETRY OF THE MACHINE

The design of electric machines is not only an art but also a science [18]. The TFPMG geometry proposed in this paper for one phase of generator is illustrated in Fig. 1. The stator is formed by the armature winding, U-cores, and I-cores. The rotor, on the other hand, consists of the rotor yoke which has Permanent Magnets (PM) attached to its surface.

The machine shown in Fig. 1 has 20 poles, each pair of poles is formed by a U-core, an I-core and two portions of the rotor of two PM each. Besides, each of these pieces have an outer diameter of the rotor, D_{er} . Additionally, in Fig. 2 it is displayed a pair of poles with their magnetic symmetry and the path of magnetic flux which is denominated transverse flux. This geometry will be modeled using 3D-FEM and the results will be compared with the results obtained with the analytical equations.

As can be seen in Fig. 2 the rotor with attached PM on the surface, has two rings. Furthermore, the consequent PM are perfectly aligned one opposite the other.

TABLE 1. Novelties of this work compared to other reviewed papers.

Previous papers [1]	In this work	References
Motor.	Generator.	[1]–[5], [9].
Medium tension, MW, non-iterative algorithm, and 2D-FEM.	Standardized low tension, kW, iterative algorithm, reluctance circuit, and 3D-FEM.	[10], [21].
Wind turbines.	Sea waves or small-scale hydroelectric turbines.	[6], [8]–[11], [13], [19], [23], [24].
Wave and tidal mechanism, very large external diameter of the rotor (6 m), efficiency less than 90%, Amperè’s law, does not indicate induced emf or terminal voltage.	Sea waves or small-scale hydroelectric turbines, the external diameter of the rotor calculated considering the cross-section of the U-core, known terminal voltage.	[12], [22].
Design guidelines.	Detailed design.	[7], [9], [10], [13], [18]–[21], [24].
Low tension and very low tension.	Standardized low tension.	[14]–[16], [21].
Without FEM.	Using 3D-FEM.	[1], [4], [8], [9].
U-core with rectangular or square cross-sections.	U-core with elliptical cross-sections.	[13], [15], [16].
No information.	U-core and I-core not considering the total extension of the polar pitch.	
Rectified trajectories of flux tubes were used to model the leakage magnetic flux.	Curved trajectories of flux tubes were used to model the leakage magnetic flux.	[26].

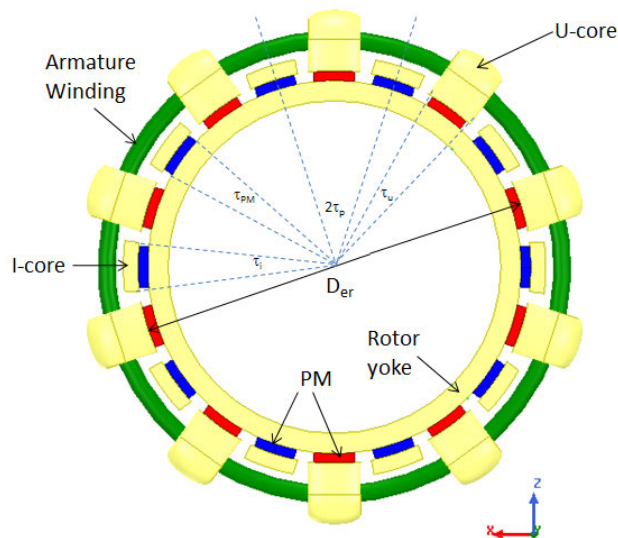


FIGURE 1. Topology of the TFPMG.

An important magnitude for the symmetric distribution of the rotor and stator elements is the pole pitch angle (τ_p), see Fig. 1. Such angle is determined considering the number of

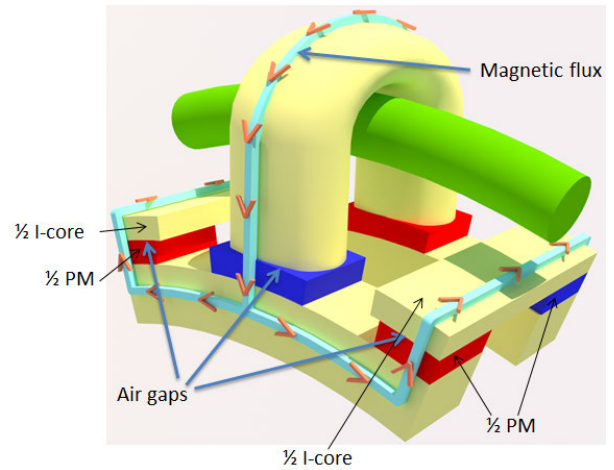


FIGURE 2. Magnetic symmetry for a pair of poles.

pole pairs (p), as indicated in eq. (1):

$$\tau_p = \frac{360^\circ}{2p}. \tag{1}$$

The angle that includes every PM of the pole pitch (τ_{PM}) is determined with the constant k_{PM} , shown in eq. (2):

$$\tau_{PM} = k_{PM} \tau_p. \tag{2}$$

The value of such constant, of machines with radial flux topology, varies between 0.66 and 1 [17], [19]. This consideration is assumed as valid in the design proposed, since in the analyzed literature, concerning transverse topology machine nothing is mentioned about the accompanying values of the PM polar pitch [1], [7], [9], [10], [13], [15], [17]–[19], moreover, the rotor magnetic circuit has the same functionality as machines with radial flux topology. Thus, the rotors have the PM attached to the surface or buried, supplying through the PM the excitation of the magnetic field, and by the rotor yoke a closed high permeability way for the circulation of the main magnetic flux.

Figure 1 shows the characteristics angles for the TFPMG that are intended to size in the present work. In Fig. 3 it is presented all the remaining dimensions for the magnetic symmetry of a pair of poles of TFPMG, plus its magnetic circuit considering an infinite permeability core, without considering leakage fluxes.

B. ROTOR DIMENSIONS

To design the rotor, it is used a Torque per Volume unit methodology, TRV [17]. Such methodology establishes the following:

$$TRV = 2\sigma_{Ftan}, \tag{3}$$

where σ_{Ftan} is the tangential stress of the rotor surface. The magnitude for synchronous machines cooled with air, may vary from 19 to 59.5 kPa [18]. Thus, the V_r volume where such torque is exerted is a volume of the imaginary cylinder

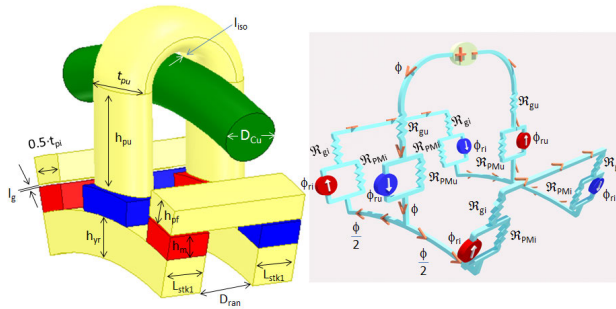


FIGURE 3. Dimensions of a pair of poles and reluctance circuit.

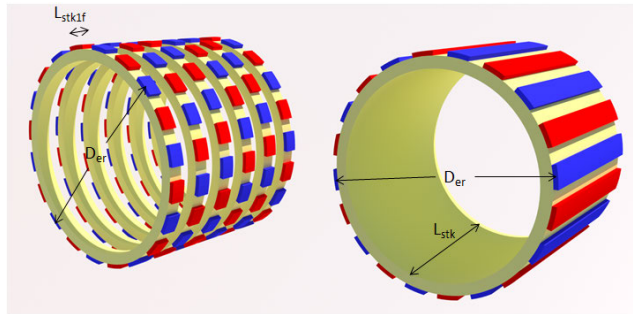


FIGURE 4. Decomposition of a 3-phase rotor.

where it is geometrically registered as a solid rotor. Such an imaginary cylinder with a D_{er} diameter (see Fig. 1) is projected along with the magnitude of the axial length (L_{stk}) of the machine. Therefore, the torque per volume unit, TRV, is executed by this solid rotor, with a D_{er} diameter and L_{stk} axial length. However, is required more information to obtain the external diameter of the rotor and the axial length of the machine. The torque is implicit in the nominal values of the machine, the tangential stress is a value known by the designer. From eq. (3) it is possible to determine the V_r volume rotor. Then, it is needed to consider that the relation of the axial length and the external diameter of the rotor k_{DL} [13], [17], [19], [23] is as indicated in eq. (4), which is a value selected by the designer.

$$0.1 < \left(k_{DL} = \frac{L_{stk}}{D_{er}} \right) < 0.27. \quad (4)$$

Thus, it is possible to determine the outer diameter of the rotor (D_{er}) as indicated:

$$D_{er} = \frac{4}{\pi} \sqrt[3]{\frac{4V_r}{\pi k_{DL}}}, \quad (5)$$

where the factor $\frac{4}{\pi}$ is proposed by the authors, corresponding to the relation between rectangular cross-section and elliptical cross-section. The latter is aimed at moving the external rotor away to make the elliptic cross-sections of the U-cores more robust. Then, the result of eq. (5) and considering the previously mentioned k_{DL} in eq. (4), it is possible to determine the total axial length of the rotor (L_{stk}) which will allow

determining the axial length of every portion of the rotor, considering the number of phases of the machine (m).

$$L_{stk1} = \frac{L_{stk}}{2m}. \quad (6)$$

The value obtained in eq. (6) is possible to be seen in Fig. 3 and Fig. 4. The height of PM (h_m) is a choice of the designer and the height of the rotor yoke (h_{yr}) will be calculated from the resolution of the magnetic circuit indicate in Fig. 3, as it is necessary to know the value of the air gap magnetic flux, ideally, divided into two parts in the rotor yoke. Thus, the magnetic circuit in Fig. 3 it is necessary to consider that is the reluctance of a PM in front of a U-core, with a surface is S_{PM} , \mathfrak{R}_{PMi} is the reluctance of a PM in front of an I-core, with a surface, \mathfrak{R}_{gu} is the reluctance of the air gap in front of a U-core, \mathfrak{R}_{gi} is the reluctance of the air gap in front of an I-core and its surface is half as compared to \mathfrak{R}_{gu} . \mathfrak{R}_{PMu} is the reluctance of a PM in front of a U-core, with a surface is S_{PM} , \mathfrak{R}_{PMi} is the reluctance of a PM in front of an I-core, with a surface is $\frac{S_{PM}}{2}$. ϕ_{ru} is the remanent magnetic flux of the PM in front of a U-core and ϕ_{ri} is the remanent magnetic flux of the PM in front of an I-core. For the magnetic circuit of Fig. 3 it is possible to determine the magnetic flux of the air gap, given by:

$$\phi = \frac{S_{PM}PC \left(B_r + NI \frac{\mu_0 \mu_{rec}}{4h_m} \right)}{PC + \mu_{rec}}, \quad (7)$$

where S_{PM} is the surface of a PM in front of a U-core, PC is the permeance coefficient of the PM (chosen by the TFPMG designer), B_r is the remanent flux density of the PM (given by the PM manufacturer), N is the number of turns of the winding armature (in the following sections), I is the nominal current, μ_0 is the vacuum permeability, μ_{rec} is the relative recoil permeability of each PM and h_m is the height of the PM. During this phase, to determine the magnetic flux, the designer of the TFPMG may consider or not, the coil current. The number of turns is determined at a later stage, thus, in that instance, it is possible to go back to eq. (7) and eq. (8) to correct the height of the rotor yoke:

$$h_{yr} = \frac{\phi}{2B_{yr}L_{stk1}}, \quad (8)$$

where ϕ is the value of the magnetic flux of the air gap, L_{stk1} is the length in the axial direction of the rotor yoke, and B_{yr} is the magnetic flux density in the rotor yoke. This value is chosen by the designer, along with the material. Its usual values are between 1 and 1.5 T [18].

C. AIR GAP

The air gap length of the machine (l_g) is determined by two designing factors, namely the height of the PM (h_m) and the permeance coefficient of the PM (PC), see eq. (9) [17]:

$$l_g = \frac{h_m}{PC}. \quad (9)$$

The air gap, eq. (9), it is not obtained in the same way as in [24].

D. ELECTROMOTIVE FORCE

The definition of electromotive force is related to the equivalent circuit by phase of a synchronous machine and it is given by:

$$E_a = k_{E_a} V, \quad (10)$$

where k_{E_a} is a constant value chosen by the designer of the generator; $1 < k_{E_a} \leq 1.4$, and V is the nominal voltage per phase. In the concentrated parameters models for synchronous machines, the electromotive force is no more than 1.4 times the base voltage per unit [25].

Now, it is determined the linked flux of the armature coil (λ_0):

$$\lambda_0 = \frac{E_a}{\omega_s p^2}, \quad (11)$$

where E_a is the electromotive force of one phase of the generator, defined in eq. (10), ω_s is the angular velocity and p is the number of pole pairs of the TFPMG. The linked flux for the armature winding is calculated to determine its number of turns, determining in the first place an initial number of turns $N^{(0)}$:

$$N^{(0)} = Integer_{greater} \left(\frac{\lambda_0}{\phi^{(0)}} \right). \quad (12)$$

In eq. (12) the magnetic flux must be evaluated according to eq. (7) considering $I = 0$ and this result will be noted as $\phi^{(0)}$. Then, an iterative process begins to obtain the total number of turns, as indicated in Fig. 5.

Now, it is defined the electromotive force E_a :

$$E_a = (1 - k_{disp}) \omega_s p^2 N \phi, \quad (13)$$

where k_{disp} is a per-unit value that indicates the magnetic flux quantity which leaks along the trajectory of each pair of poles of the TFPMG, chosen by the designer.

If eq. (13) is evaluated with $N^{(0)}$, see eq. (12), it is obtained $E_a^{(0)}$. Thus, it is possible to pose the following iterative process, starting with $\phi^{(0)}$, $N^{(0)}$ and $E_a^{(0)}$. The iterative process proposed is shown in Fig. 5. Once the iterative process converges, it is possible to update the rotor yoke value h_{yr} in eq. (8).

E. WIRES AND SLOTS

To characterize the armature-coil conductors, firstly it is necessary to calculate the winding currents since such current determines the section of the conductors. This current is calculated by:

$$I = \frac{P}{\sqrt{3} V \cos \varphi}, \quad (14)$$

where P is the power of the TFPMG, V is the voltage in the generator terminals and $\cos \varphi$ is the nominal power factor. The values indicated are designing values, which are intended to verify in the proposed designing guidelines.

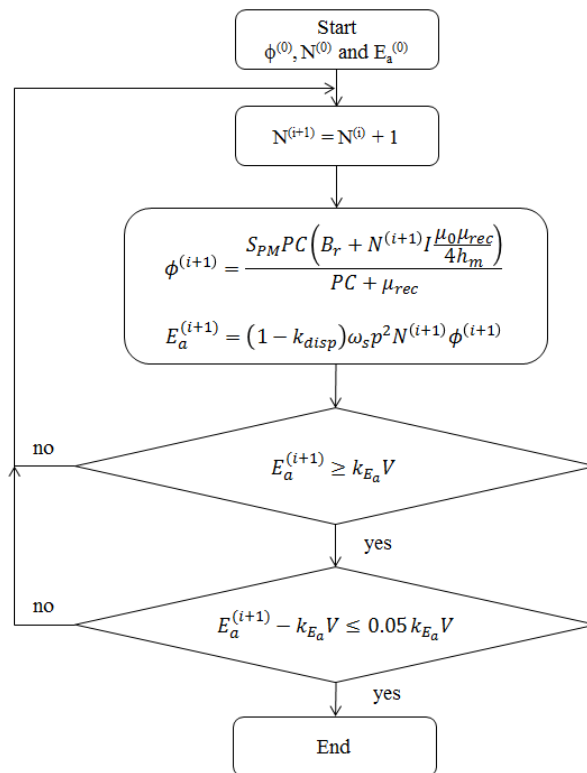


FIGURE 5. Iterative process flow diagram.

The conductors of the armature winding housed in the slot, have a cross-section S_c which will be determined by eq. (15):

$$S_c = \frac{I}{J}, \quad (15)$$

where I is the nominal current of the TFPMG, and J is the current density of the conductors housed in the slot. In air-cooled synchronous machines, the current density is a value between 4 and 6.5 A/mm² [18].

As it is a low voltage machine, the armature winding has a ring form, and it is supposed that the conductors have a circular cross-section. Thus, the conductor diameter is given by:

$$D_c = \sqrt{\frac{4}{\pi} S_c}. \quad (16)$$

With the results obtained from eq. (15) it is possible to determine the quantity of copper in the slots. The cross-section of the slot is given by:

$$S_{Cu} = N S_c. \quad (17)$$

Therefore, it is possible to determine the equivalent diameter of copper in the slots:

$$D_{Cu} = \sqrt{\frac{4}{\pi} S_{Cu}}. \quad (18)$$

Then, with the equivalent diameter conductor D_{Cu} determined by eq. (18) it is possible to define an isolation safety distance l_{iso} that jointly define the slot diameter. The slot

diameter D_{ran} obtained by eq. (19) and the component that forms D_{Cu} and l_{iso} are shown in Fig. 3.

$$D_{ran} = D_{Cu} + 2l_{iso}. \quad (19)$$

Finally, the total area of the slot S_{slot} is calculated based on the diameter of the slot D_{ran} :

$$S_{slot} = \frac{D_{ran}^2}{4} \frac{\pi}{k_{slot}}. \quad (20)$$

In the total area of the slot S_{slot} indicated in eq. (20) it can be seen that it is filled with copper from the armature winding and also with air, that is why that factor k_{slot} is considered, which varies from 0.4 and 0.6 [19]. The air is necessary for ventilation purposes.

F. CORES

In this section, it is calculated the size that characterizes the U-cores and I cores, according to what is shown in Fig. 3.

In the same way that it is calculated in the angle range, every PM from the pole pitch. The present research proposes as an innovation, that the U-cores and I-cores could partially accompany the pole path. Thus, the angles τ_u and τ_i , shown in Fig 1, are the fractions of the pole path that accompanies each core. These angles are determined by:

$$\tau_u = k_{nu}\tau_p, \quad (21)$$

$$\tau_i = k_{ni}\tau_p, \quad (22)$$

where k_{nu} and k_{ni} are the accompanying fraction of the pole pitch. It is a constant number and less than 1.

The depth of the U-core, t_{pu} is a chord of the angle arc τ_u , immediately after the air gap:

$$t_{pu} = (D_{er} + 2l_g) \sin \frac{\tau_u}{2}. \quad (23)$$

Similarly, it is possible to calculate the depth of the I-core:

$$t_{pi} = (D_{er} + 2l_g) \sin \frac{\tau_i}{2}. \quad (24)$$

In eq. (23) and eq. (24), D_{er} is the outer diameter of the rotor, l_g is the height of the air gap, τ_u is the angle of a U-core that accompanies the pole pitch, and τ_i is the angle of an I-core that accompanies the pole pitch.

Now, it is possible to determine the height of the leg parts of the U-core, h_{pu} :

$$h_{pu} = \frac{S_{slot}}{D_{ran}} - \frac{D_{ran}}{8} \pi, \quad (25)$$

where S_{slot} is the total area of a slot and D_{ran} is de diameter of the slot of the separation of the U-core legs.

Finally, the height of each I-core (h_{pi}) is determined by:

$$h_{pi} = \frac{2\phi}{B_{pi} (D_{er} + 2l_g) \tau_i}, \quad (26)$$

where ϕ is the magnetic flux, B_{pi} is the magnetic flux density in the I-core, D_{er} is the external diameter of the rotor, l_g is the air gap, and τ_i is the angle of the i-core that accompanies the pole pitch.

For design purposes, it is suggested to consider that an I-core is equivalent to a stator yoke, thus, the magnetic flux density can be between 1 and 1.5 T [18], a value that is chosen during the design phase.

III. LUMPED PARAMETERS OF THE TFPMG

In the topology that the rotor presents, with PM attached to the surface, it is possible to consider that the air gap is uniform, as the relative coil permeability μ_{rec} of the PM is a dimensionless value extremely close to one. Thus, the passive elements of the TFPMG can be characterized by the resistance of the armature R_a a synchronous inductance L_s in series, as traditional in synchronous machines of smooth rotors.

A. ARMATURE RESISTANCE

The resistance of the armature is characterized by the average diameter of the ring of the N-turn copper conductors:

$$R_a = \frac{N (D_{er} + 2l_g + 2h_{pu}) \pi}{\sigma_{Cu} S_c}, \quad (27)$$

where N is the number of turns of the armature coil, D_{er} is the rotor external diameter, l_g is the air gap, h_{pu} is the leg height of the U-core, σ_{Cu} is the copper conductivity and S_c is the cross section of a conductor housed in the slot.

B. SYNCHRONOUS INDUCTANCE

To determine the synchronous inductance L_s , it should be considered as a first base the ideal magnetic circuit of Fig. 3. When observing such a circuit, it will be considered the geometry of the pieces, their separation, and localization. Thus, the reluctances are inserted and they represent the leakage flux trajectories, very similar to what is shown in [26] but we have considered the curvatures of some of their trajectories. Then, the new reluctance network is established as indicated in Fig. 6. In that figure and as compared to the ideal magnetic circuit of Fig. 3 four reluctance elements are inserted expecting that the trajectories that will consider the magnetic flux leakage will be established.

When circulating through the armature winding, the first trajectory to consider is the right-hand rule and will be the first reluctance leakage \mathfrak{R}_1 through all the legs height of the U-core:

$$\mathfrak{R}_1 = \frac{D_{ran}}{\mu_0 D_{ran} t_{pu}}. \quad (28)$$

The second trajectory takes into consideration that the leakage magnetic flux is a magnetic flux that leaks out of the U-core legs, from both end faces. Thus, \mathfrak{R}_2 is defined as:

$$\mathfrak{R}_2 = \frac{1}{\mu_0 h_{pu}} \left(\frac{\pi}{2 \ln 2} + \frac{2D_{ran}}{t_{pu}} \right). \quad (29)$$

In eq. (28) and eq. (29), D_{ran} is the slot diameter, μ_0 is the vacuum permeability, t_{pu} is the width of one leg of the U-core, and h_{pu} is the leg height of the U-core.

The insertion of \mathfrak{R}_1 and \mathfrak{R}_2 in the reluctance network, and the magnetic flux leakage paths can be observed in part (a)

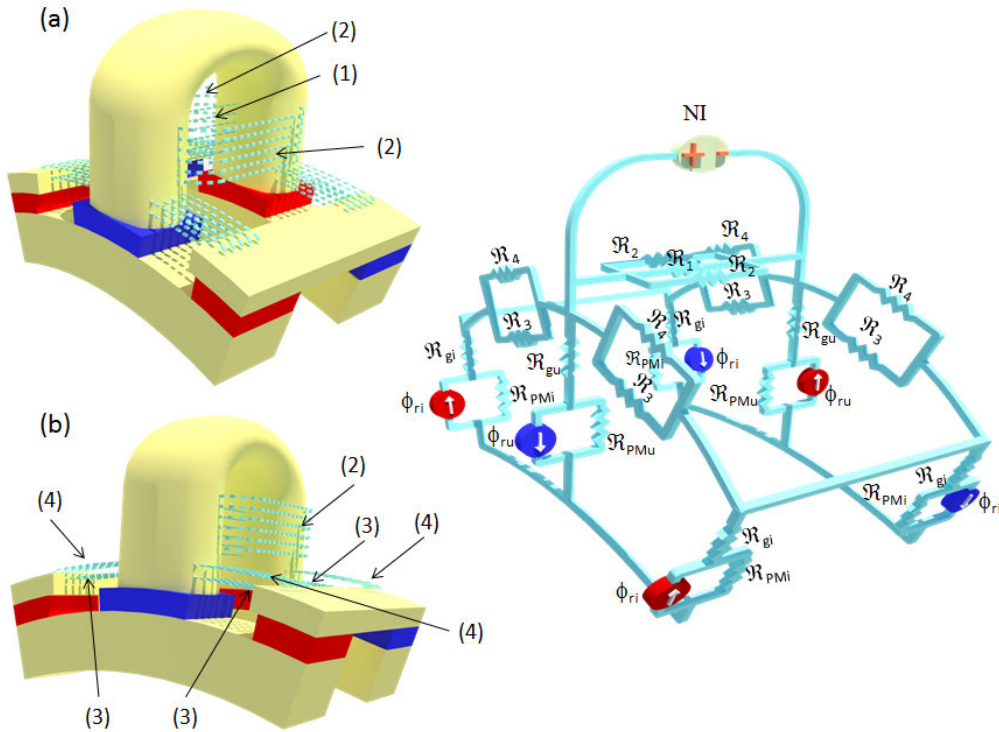


FIGURE 6. Leakage flux paths and reluctance circuit to the TFPMG topology.

of Fig. 6. Thus, three reluctances appear in parallel under the magneto-motive force found of the armature winding.

Now, between the U-core and the I-core two leakage trajectories can be considered. One trajectory between the end faces of the U-core and the I-core, thus it is possible to determine \mathfrak{R}_3 as:

$$\mathfrak{R}_3 = \frac{\left(1 - \frac{k_{nu}}{2} - \frac{k_{ni}}{2}\right) \tau_p}{\mu_0 L_{stk1} \ln\left(1 + \frac{2h_{pi}}{D_{er} + 2l_g}\right)}. \quad (30)$$

The second trajectory of the magnetic flux leakage to consider, goes from one leg of the U-core, parallel and under the armature winding, falling from the superior part of the I-core. Thus, \mathfrak{R}_4 is determined as follows:

$$\mathfrak{R}_4 = \frac{\pi + (2 - k_{nu} - k_{ni}) \tau_p}{2\mu_0 L_{stk1} \ln\left(1 + \frac{2L_{stk1}}{D_{er} + 2l_g + 2h_{pi}}\right)}. \quad (31)$$

In eq. (30) and eq. (31), k_{nu} is the accompanying fraction of the U-core pole pitch, k_{ni} is the accompanying fraction of the I-core pole pitch, τ_p is the pole pitch, μ_0 is the vacuum permeability, is the length of the axial direction of the rotor yoke, D_{er} is the rotor external diameter, l_g is the air gap and h_{pi} is the I-core height.

In the reluctance network, the leakage fluxes indicated in part (b) of Fig. 6 are represented by reluctances \mathfrak{R}_3 and \mathfrak{R}_4 . Thus, in the symmetry of a pair of poles, such reluctances

are parallel and located symmetrically in the network. Each is four times as indicated in the reluctance network of Fig. 6.

To determine the total inductance value of the machine, it is necessary to know the air gap and PM reluctance. The topology has two air gaps facing the PM and U-core, the reluctance of each air gap, in front of the U-core, \mathfrak{R}_{gU} is determined by eq. (32):

$$\mathfrak{R}_{gU} = \frac{2l_g}{\mu_0 k_{PM} \tau_p (D_{er} + 2l_g) L_{stk1}}. \quad (32)$$

Four air gaps face the I-cores with the PM in the pair of poles symmetry, see Fig. 6, such air gaps have a cross-section that is half of the air gap area which faces the U-Core with the PM. The reluctance of each air gap under the I-cores \mathfrak{R}_{gi} is determined by eq. (33):

$$\mathfrak{R}_{gi} = \frac{4l_g}{\mu_0 k_{PM} \tau_p (D_{er} + 2l_g) L_{stk1}} = 2\mathfrak{R}_{gU}. \quad (33)$$

In eq. (32) and eq. (33), l_g is the air gap height, μ_0 is the vacuum permeability, k_{PM} is the accompanying fraction of the PM pole pitch, τ_p is the pole pitch, D_{er} is the rotor external diameter and L_{stk1} is the length in the axial direction of the rotor yoke.

The PM reluctancies under the U-core \mathfrak{R}_{PMU} are determined by eq. (34):

$$\mathfrak{R}_{PMU} = \frac{2h_m}{\mu_0 \mu_{rec} k_{PM} \tau_p D_{er} L_{stk1}}. \quad (34)$$

Finally, the PM reluctances under the I-core \mathfrak{R}_{PMi} are indicated in eq. (35). Similarly, concerning the cross-sections of the air gaps under the I-cores and U-cores, the relation is the same. So, they have the same reluctance relation ($\mathfrak{R}_{PMi} = 2\mathfrak{R}_{PMU}$):

$$\mathfrak{R}_{PMi} = \frac{4h_m}{\mu_0\mu_{rec}k_{PM}\tau_p D_{er}L_{stk1}} = 2\mathfrak{R}_{PMU}. \quad (35)$$

In eq. (34) and eq. (35), h_m is the PM height, μ_0 is the vacuum permeability, μ_{rec} is the relative recoil permeability, k_{PM} is the accompanying fraction of the PM pole pitch, τ_p is the pole pitch, D_{er} is the rotor outer diameter and L_{stk1} is the length in the axial direction of the rotor yoke.

As stated in eq. (28) up to eq. (34) the reluctance network is characterized, a least, by the passive elements of its circuit. Thus, with delta-star transformations and parallel-series reduction, it is possible to calculate the Thevenin equivalent reluctance \mathfrak{R}_{th} in the terminals of the armature winding, source of the magnetomotive force, that with the number of pole pairs p and the number of turns N resulting from the iterative process of Fig. 5, it is possible to obtain the synchronous inductance L_s as shown in eq. (36):

$$L_s = \frac{N^2}{\mathfrak{R}_{th}} p. \quad (36)$$

IV. EFFICIENCY, VOLUME, AND MASS

In this section it is proposed a methodology to calculate the efficiency and losses, incorporating the IEC 60034-2-1 [21] standard for the segregation of the power losses. Finally, it is indicated the guidelines to determine the TFPMG volume and mass.

A. EFFICIENCY

The performance calculation can be done as indicated by eq. (37) [21]:

$$\eta = \frac{P_L}{P_L + P_S + P_{LL} + P_{Fe}} 100\%. \quad (37)$$

where P_L is the power load of the generator, P_S are the stator winding losses, P_{LL} are the additional-load losses, and P_{Fe} are the core losses. Thus, it is possible to calculate each component of eq. (37) as follows. Firstly, the power load of the generator is calculated by:

$$P_L = 3V_{1\phi}I\cos\varphi, \quad (38)$$

where $V_{1\phi}$ is the voltage per phase of the generator, I is the armature current and $\cos\varphi$ is the power factor.

Now, the stator winding losses are calculated by:

$$P_S = 3I^2R_a, \quad (39)$$

where I is the armature current, and R_a is the armature resistance.

According to [18], [21] the additional-load losses are determined by the assignation method:

$$P_{LL} = k_{LL}P, \quad (40)$$

TABLE 2. Correction factors and other parameters to determine total core losses.

Symbol	Magnitude	Unit
$k_{Fe,legU}$	2.0	
$k_{Fe,arcU}$	1.6	
$k_{Fe,I}$	1.6	
$P_{1,5}$	1.1	W/kg
m	3	
p	10	

where k_{LL} is the loss assignation constant which goes from 0.001 to 0.002 [18], [21], and P is the nominal power of the generator.

The total core losses P_{Fe} , eddy and hysteresis, are determined as indicated in [18] but considering the magnetic circuit topology of the machine and the magnetic flux densities that are expected to obtain:

$$P_{Fe} = \sum_n k_{Fe,n} P_{1,5} \left(\frac{B_n}{1.5 [T]} \right)^2 m_{Fe,n}, \quad (41)$$

where $k_{Fe,n}$ is a correction factor for synchronous machines [18], $P_{1,5}$ is the material loss density in W/kg for 1.5 T, B_n the magnetic flux density from the part of the generator in which the core losses are evaluated and $m_{Fe,n}$ is the mass of the generator part in which core losses are evaluated. Particularly, for calculation purposes, the U-core is segregated in two columns and an arc.

Then, for this case the total core losses, eddy and hysteresis, P_{Fe} are expressed as:

$$P_{Fe} = (2k_{Fe,legU} P_{1,5} \left(\frac{B_1}{1.5 [T]} \right)^2 m_{Fe,legU} + k_{Fe,arcU} P_{1,5} \left(\frac{B_2}{1.5 [T]} \right)^2 m_{Fe,arcU} + k_{Fe,I} P_{1,5} \left(\frac{B_4}{1.5 [T]} \right)^2 m_{Fe,I}) pm, \quad (42)$$

where $k_{Fe,legU}$ is a correction factor for a leg of the U-core, $P_{1,5}$ is the material loss density in W/kg for 1.5 T, B_1 is the magnetic flux density in a leg of the U-core (see Fig. 8), $m_{Fe,legU}$ is a leg mass of the U-core, $k_{Fe,arcU}$ is a correction factor for a U arc of the U-core, B_2 is the magnetic flux density in a U arc of the U-core (see Fig. 8), $m_{Fe,arcU}$ is the U arc mass of the U-core, $k_{Fe,I}$ is a correction factor for the I-core, B_4 is the magnetic flux density in a I-core (see Fig. 8), $m_{Fe,I}$ is a I-core mass, p is a pair poles and m is the number of phases.

To evaluate the eq. (42) the values shown in table (2) must be considered.

B. VOLUME

According to the geometry and angles shown in Fig. 1 and Fig. 3 the expressions for the volume are presented. The volume of an U-core V_U , is expressed as the sum of the

volume of one leg plus the arc volume of the U:

$$V_U = \frac{\pi}{2} L_{stk1} t_{pu}^2 + \frac{\pi^2}{8} (D_{ran} + L_{stk1}) L_{stk1} t_{pu}. \quad (43)$$

Although eq. (43) can be reduced a little further, it has not been done since the first term represents the volume of two legs of the U-core and the second term represents the arc volume of the U-core. In eq. (43) L_{stk1} is the length in the axial direction of the rotor yoke, t_{pu} is the width of one leg of the U-core, and D_{ran} is the slot diameter.

The volume of one I-core is determined by:

$$V_I = \frac{\tau_i}{4} \left(\left(\frac{D_{er}}{2} + l_g + h_{pi} \right)^2 - \left(\frac{D_{er}}{2} + l_g \right)^2 \right) (D_{ran} + 2L_{stk1}), \quad (44)$$

where τ_i is the accompanying angle of pole pitch of an I-core, D_{er} is the external diameter of the rotor, l_g is the air gap, h_{pi} is the height of an I-core and L_{stk1} is the length in the axial direction of the rotor yoke.

The volume of the armature winding is:

$$V_w = 2\pi \left(\frac{D_{er}}{2} + l_g + h_{pu} \right) S_{Cu}, \quad (45)$$

where D_{er} is the external diameter of the rotor, l_g is the air gap, h_{pu} is the height of one leg of the U-core, and S_{Cu} is the total copper area of the slot.

Now, it is necessary to determine the volume of the rotor parts and the volume of the permanent magnet is obtained as follows:

$$V_{PM} = \frac{\tau_{PM}}{2} \left(\left(\frac{D_{er}}{2} \right)^2 - \left(\frac{D_{er}}{2} - h_m \right)^2 \right) L_{stk1}, \quad (46)$$

where τ_{PM} is the accompanying angle of a pole pitch of a PM, D_{er} is the external outer diameter, h_m is the height of a PM and L_{stk1} is the length in the axial direction of the rotor yoke.

Finally, the volume of a pole pitch of one of the yoke rotors is:

$$V_{ly} = \frac{\tau_p}{2} \left(\left(\frac{D_{er} - h_m}{2} \right)^2 - \left(\frac{D_{er}}{2} - h_m - h_{yr} \right)^2 \right) L_{stk1}, \quad (47)$$

where τ_p is the pole pitch angle, D_{er} is the external outer diameter, h_m is the height of a PM, h_{yr} is the height of the rotor yoke and L_{stk1} is the length in the axial direction of the rotor yoke.

Thus, the total volume of a TFPMG is:

$$V_{TFPMG} = m (p (V_U + V_I + 4V_{PM} + 2V_{ly}) + V_w), \quad (48)$$

where m is the number of phases, p are the pairs of poles, V_U is the U-core volume, V_I is the I-core volume, V_{PM} is the PM volume, V_{ly} is the rotor yoke volume and V_w is the armature winding volume.

TABLE 3. Parameter data of TFPMG.

Parameter	Symbol	Magnitude	Unit
Power	P	10	kW
Voltage	V	380	V
Voltage per phase	$V_{1\phi}$	220	V
Power factor	$\cos\varphi$	1	
Number of phases	m	3	
Pole pairs	p	10	
Frequency	f	50	Hz

TABLE 4. Permanent magnet data.

Parameter	Symbol	Magnitude	Unit
Remanent flux density	B_r	1.2	T
Permeance Coefficient	PC	10	
Magnet height	h_m	5	mm
Relative recoil permeability	μ_{rec}	1.1	

C. MASS

To determine the TFPMG mass, it is used the material densities of each component of the generator. Thus, the mass can be determined as follows:

$$M_g = m (p (\rho_{Fe} (V_U + V_I + 2V_{ly}) + 4\rho_{PM} V_{PM}) + \rho_{Cu} V_w), \quad (49)$$

where m is the number of phases, p is for the pairs of poles, ρ_{Fe} is the core density, V_U is the U-core volume, V_I is the I-core volume, V_{ly} is the rotor yoke volume, ρ_{PM} is the PM density, V_{PM} is the volume of a PM, ρ_{Cu} is the copper density and V_w is the armature winding volume.

V. TFPMG DESIGN

To design the generator, it is necessary to choose electric, magnetic, and mechanic variables which define its performance. Table (3) presents the parameter data of TFPMG.

TABLE 5. Design values.

Parameter	Symbol	Magnitude	Unit
Tangential stress	σ_{Flan}	17	kPa
Current density	J	5.25	A/mm ²
Rotor yoke flux density	B_{yr}	1.10	T
I-core flux density	B_{pi}	1.15	T
EMF factor	k_{Ea}	1.25	
Leakage factor	k_{disp}	0.25	
Width PM factor	k_{PM}	0.85	
Axial length relation to the diameter	k_{DL}	0.20	
Slot filling factor	k_{slot}	0.50	
Width U-core factor	k_{nu}	0.90	
Width I-core factor	k_{ni}	0.90	
Slot insulation	l_{iso}	1	mm

Table (4) shows the PM specifications used in the design and which represent the generator field-circuit. Then, the table (5) displays the designing values of the mechanics, electromagnetic and geometric variables that will allow designing the machine parts, as indicated in sections 2 and 3.

TABLE 6. Design analytical results.

Symbol	Result	Unit	equation
τ_p	18	degrees	1
τ_{PM}	12	degrees	2
TRV	34	Nm/m^3	3
D_{er}	497.35	mm	5
L_{stk1}	16.58	mm	6
ϕ	1.19	mWb	7
h_{yr}	32.63	mm	8
l_g	0.50	mm	9
E_a	275	V	10
λ_0	875.35	mWb-turns	11
E_a	277.62	V	13 and fig. (5)
N	99	turns	fig. (5)
I	15.15	A	14
D_{Cu}	19.07	mm	18
D_{ran}	21.07	mm	19
τ_u	16.20	degrees	21
τ_i	16.20	degrees	22
t_{pu}	70.22	mm	23
t_{pi}	70.22	mm	24
h_{pu}	28.23	mm	25
h_{pi}	14.69	mm	26
R_a	1.030	Ω	27
\mathfrak{R}_1	1.13×10^7	1/H	28
\mathfrak{R}_2	5.84×10^7	1/H	29
\mathfrak{R}_3	2.63×10^7	1/H	30
\mathfrak{R}_4	1.26×10^9	1/H	31
\mathfrak{R}_{gU}	3.60×10^5	1/H	32
\mathfrak{R}_{gi}	7.21×10^5	1/H	33
\mathfrak{R}_{PMU}	3.29×10^6	1/H	34
\mathfrak{R}_{PMi}	6.57×10^6	1/H	35
L_s	28.31	mH	36
η	91.49	%	37
P_L	10.00	kW	38
P_S	708.25	W	39
P_{LL}	15.00	W	40
P_{Fe}	207.09	W	41
V_U	11.00×10^{-4}	m^3	43
V_I	2.89×10^{-4}	m^3	44
V_w	4.98×10^{-4}	m^3	45
V_{PM}	4.45×10^{-6}	m^3	46
V_{1y}	3.86×10^{-5}	m^3	47
V_{TFPMG}	85.00×10^{-4}	m^3	48
M_g	70.34	kg	49

Finally, the geometric, electromagnetic, and performance dimensions of the TFPMG are presented in the table (6).

VI. COMPARISON WITH THE FINITE ELEMENT METHOD

The comparison with the Finite Element Method (FEM) for electric machines poles with axial flux and transverse flux topologies, is only possible with three-dimensional modeling since the magnetic flux path does not present symmetric characteristics to use bi-dimensional modeling.

In the design of the TFPMG was used the 3D ANSYS® Electromagnetics Suite – Release 2020 R2 finite element software.

As for the structures, the cores of the U-core, I-core, and rotor yoke have been considered to be of Alloy – 49 material, which is included in libraries of the ANSYS®. The BH curve of the material is shown in Fig. 7. The PM was chosen with

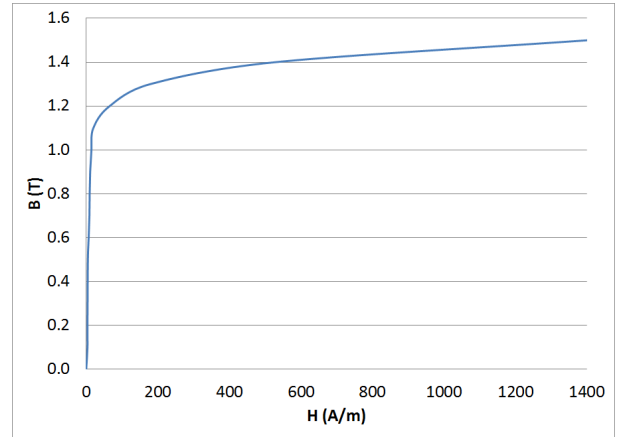


FIGURE 7. BH curve Alloy-49.

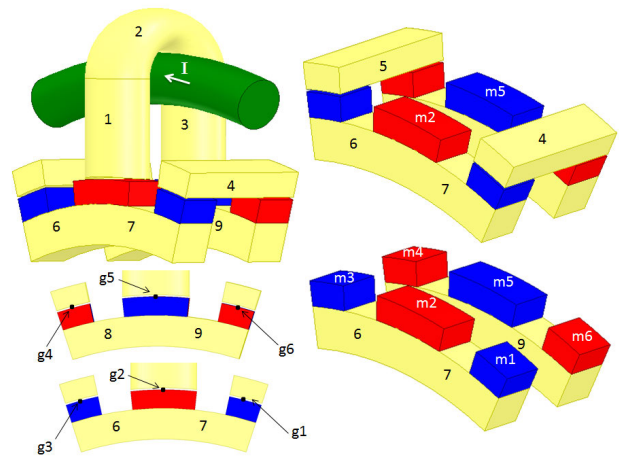


FIGURE 8. Perspective of the TFPMG and points where the Ampère law is applied.

a remanence of 1.2 T according to what was mentioned in the designing stage.

Previously, it was solved the Ampère Law, considering the non-linearity of the Alloy 49 material and posing the two closed trajectories: 1 – 2 – 3 – g5 – m5 – 8 – m4 – g4 – 5 – g3 – m3 – 6 – m2 – g2 and 1 – 2 – 3 – g5 – m5 – 9 – m6 – g6 – 4 – g1 – m1 – 7 – m2 – g2. Fig. 8 presents the points that define these two trajectories.

With the 3D finite element software, it is solved, in the first place, the magnetostatic problem to compare the magnetic flux densities, the magnetic flux, and the synchronous inductance L_s analytically obtained from the model presented in section 3.

The graphical output of the 3D finite element software is indicated in Fig. 9. Such figure presents part of the finite element network which contains 141,298 tetrahedral elements. Moreover, the diagram with the magnetic flux densities distribution and the coil current density distribution.

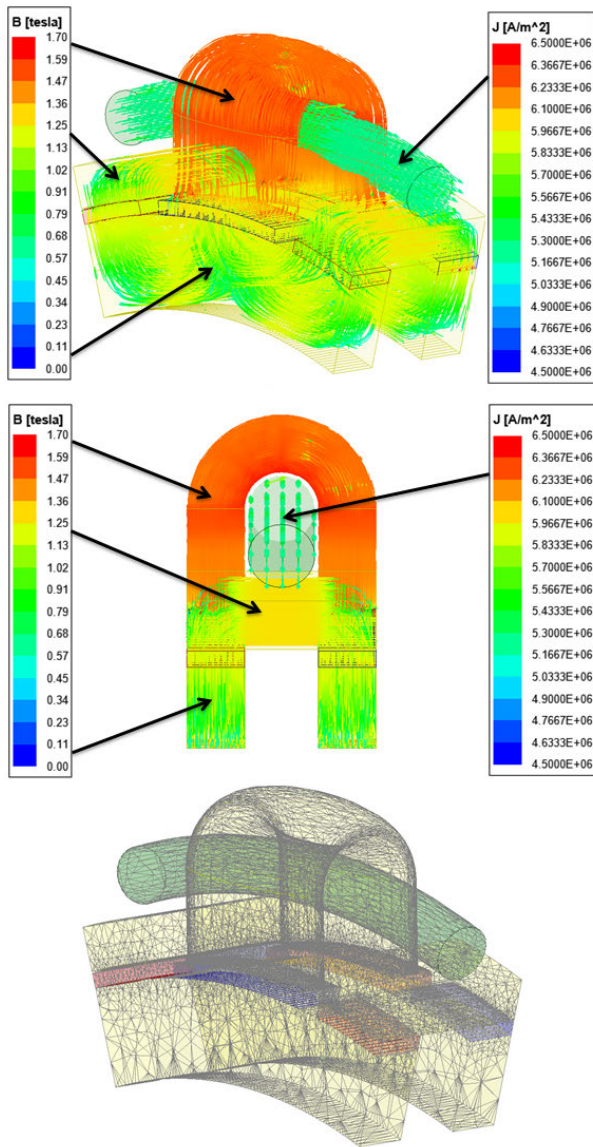


FIGURE 9. Magnetic flux density distribution, and current density distribution of the coil (top and middle images), and 3D finite element mesh (bottom image).

Both magnitudes are an output of the 3D finite element software.

Post-processing the magnetostatic calculations made by the 3D-FEM software, it is possible to compare the magnetic flux, according to the points indicated in Fig. 8, and also, the synchronous inductance L_s . This is shown in table (7). In addition, the magnetic fluxes that in table (7) have a difference greater than 10% in relation to the analytical resolution of Ampère law, show the leakage paths of the magnetic flux previously shown in Fig. 6.

Now, we move to the magnetodynamic analysis which was done with the finite element software, which allows comparing the electromotive force, see Fig. 10, the armature current, and the power losses.

TABLE 7. Analytical and 3D-FEM results.

Symbol	Unit	Analytical	3D-FEM	Difference
B_1	T	1.4261	1.3836	-3.07%
B_2	T	1.4702	1.4584	-0.81%
B_3	T	1.4261	1.3901	-2.59%
B_4	T	1.2758	1.2260	-4.06%
B_5	T	1.2758	1.2257	-4.09%
B_6	T	1.2051	1.1606	-3.83%
B_7	T	1.2051	1.1593	-3.95%
B_8	T	1.2051	1.1611	-3.79%
B_9	T	1.2051	1.1605	-3.84%
B_{g1}	T	1.1255	1.0849	-3.74%
B_{g2}	T	1.1485	1.2189	5.78%
B_{g3}	T	1.1255	1.0890	-3.35%
B_{g4}	T	1.1255	1.0839	-3.84%
B_{g5}	T	1.1485	1.2188	5.77%
B_{g6}	T	1.1255	1.0846	-3.77%
B_{m1}	T	1.1607	1.1259	-3.09%
B_{m2}	T	1.1843	1.2183	2.79%
B_{m3}	T	1.1607	1.1233	-3.33%
B_{m4}	T	1.1607	1.1242	-3.25%
B_{m5}	T	1.1843	1.2184	2.80%
B_{m6}	T	1.1607	1.1242	-3.25%
ϕ_1	mWb	1.3038	1.2668	-2.92%
ϕ_2	mWb	1.3038	1.3291	1.90%
ϕ_3	mWb	1.3038	1.2670	-2.90%
ϕ_4	mWb	0.6389	0.6319	-1.11%
ϕ_5	mWb	0.6389	0.6319	-1.11%
ϕ_6	mWb	0.6389	0.6282	-1.70%
ϕ_7	mWb	0.6389	0.6279	-1.75%
ϕ_8	mWb	0.6389	0.6289	-1.59%
ϕ_9	mWb	0.6389	0.6281	-1.72%
ϕ_{g1}	mWb	0.6389	0.5628	-13.52%
ϕ_{g2}	mWb	1.3038	1.2548	-3.91%
ϕ_{g3}	mWb	0.6389	0.5623	-13.62%
ϕ_{g4}	mWb	0.6389	0.5630	-13.48%
ϕ_{g5}	mWb	1.3038	1.2567	-3.75%
ϕ_{g6}	mWb	0.6389	0.5627	-13.54%
ϕ_{m1}	mWb	0.6389	0.5757	-10.98%
ϕ_{m2}	mWb	1.3038	1.2851	-1.46%
ϕ_{m3}	mWb	0.6389	0.5763	-10.86%
ϕ_{m4}	mWb	0.6389	0.5758	-10.96%
ϕ_{m5}	mWb	1.3038	1.2849	-1.47%
ϕ_{m6}	mWb	0.6389	0.5760	-10.92%
L_s	mH	28.3149	29.5108	4.05%

TABLE 8. Analytical and 3D-FEM Results.

Symbol	Unit	Analytical	3D-FEM	Difference
E_a	V	277.6158	266.4634	-4.19%
V_t	V	220	209.0594	-5.23%
I	A	15.1515	15.1499	-0.01%
$\cos\varphi$		1	0.9847	-1.55%
R_a	Ω	1.0284	1.2570	18.17%
P	kW	10	9.3600	-6.87%
$Losses$	kW	0.93034	0.9193	-1.20%
η	%	91.4885	91.0536	-0.48%
M_g	kg	70.3359	70.5452	0.30%

The terminal voltage, which can be seen in Fig. 11 is determined post-processing the electromotive force signal and the load current signal. The synchronous inductance (obtained by magnetostatic analysis) and the power losses analysis (which allows obtaining the coil resistance). Besides, by constructing the terminal voltage signal and plotting it with the current signal, it is possible to compare the power factor.

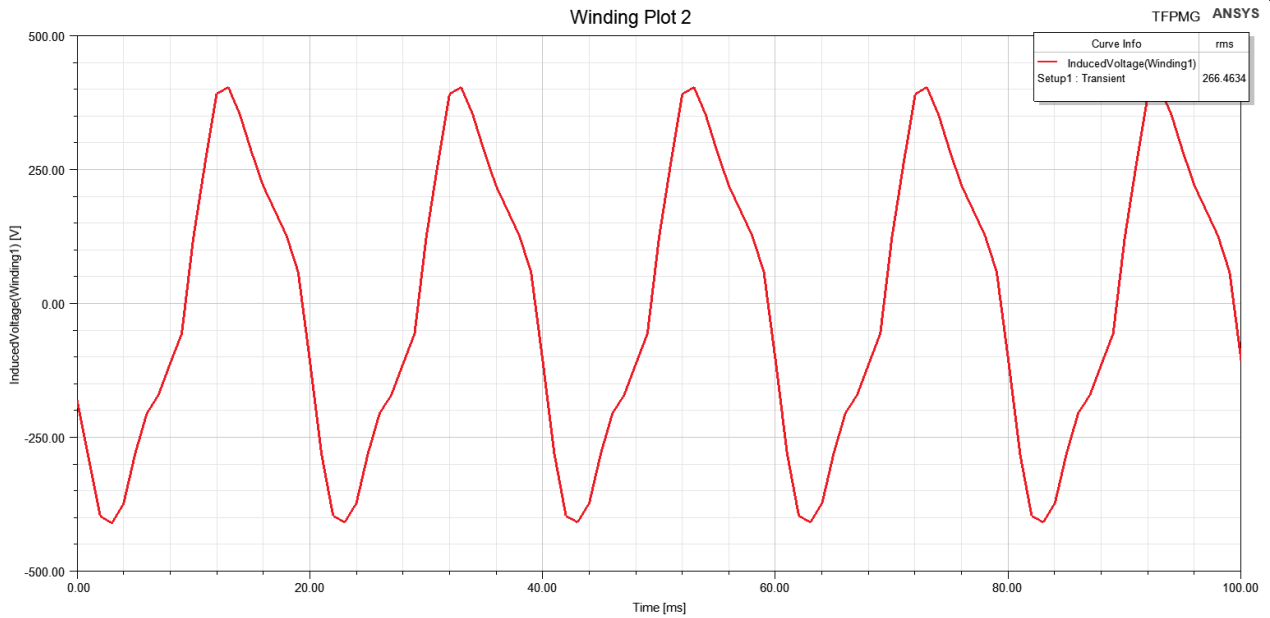


FIGURE 10. Electromotive force (per phase).

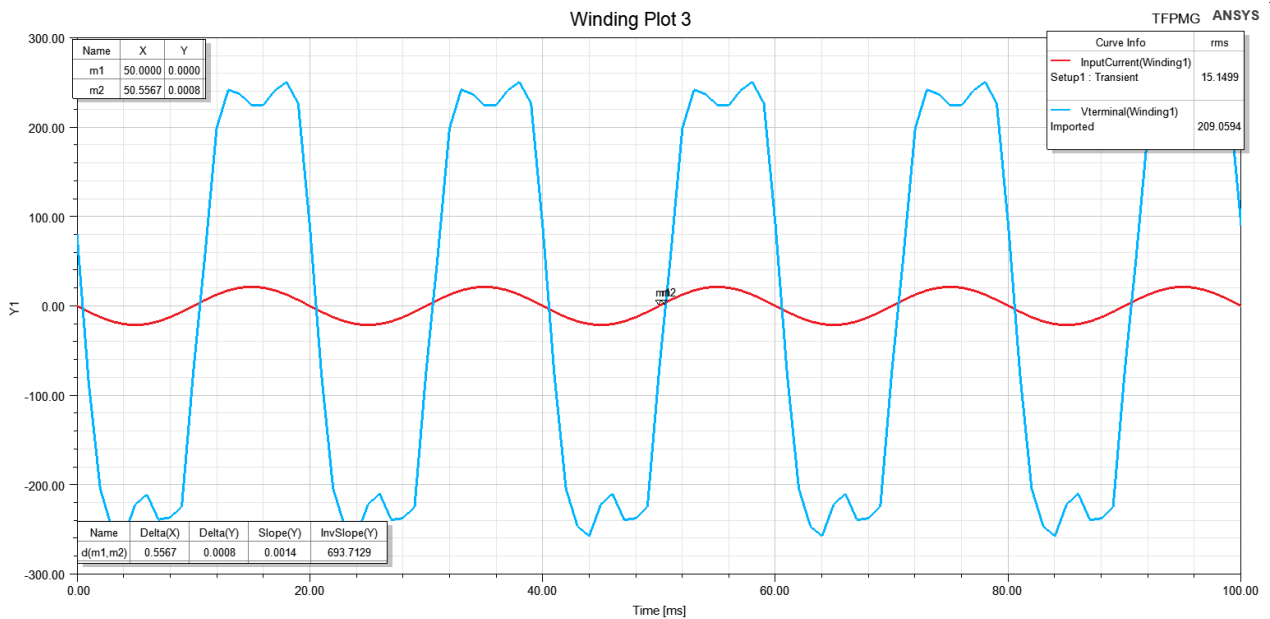


FIGURE 11. Terminal voltage (per phase) and current.

In addition, the armature current is highly resistive, simulating the generator connected to an infinite bus. Because of this, the armature current does not have harmonic distortions as if it were an isolated impedance connected directly to the armature terminals.

Thus, it is possible to calculate the load power for the voltage, current, and power factor indicated in Fig. 11. Thus, comparing it with the result of the power losses and the finite element analysis, it is also possible to compare the generator efficiency.

Finally, in tables (7) and (8) it is shown the comparison between the analytical and 3D-FEM results, comparing the design in terms of the lumped parameter, the electromagnetic performance, and the TFPMG mass.

VII. CONCLUSION

This paper has presented the design of a TFPMG, comparing the design methodology proposed with the 3D finite element analysis. Such methodology incorporates a simple, iterative model to determine the number of turns of

the armature winding, thus complying with the electromotive force specified during the designing phase. From the results obtained it is possible to verify that it is feasible to specify the terminal voltage of the machine, a fact that has been excluded by many authors according to the bibliographic review.

As for the rotor design, once the configuration is chosen, it is possible to use the same considerations for the design of an electrical machine rotor with radial magnetic flux. The latter has a significant presence in the literature available [17]–[19]. In particular, for the present work and to determine the external diameter of the rotor, it has been considered the insertion of factor $\frac{4}{\pi}$, such value is the ratio between a rectangular and elliptical cross-sections. Furthermore, the U-core and the I-core are proposed without accompanying the entire pole pitch, consequently, it is expected to use less material in the U-core and I-core just by the approach of the design methodology.

The present work carries out the comparison with a 3D-FEM. The stated considerations about magnetic flux densities, for the rotor yoke, the I-core, and the upper curved part of the U-core are compared according to the results obtained, both analytical and by FEM, the two of them are among the typical values of a yoke according to what was indicated in the design methodology. On the other hand, the magnetic flux density in front of the six air gaps included in the machine model, faces two types of geometries, but, in the worst-case situation, is a value around 1 T which is suggested in the bibliographic review.

According to the numerical validation results with 3D-FEM, it is possible to verify the magnetic flux. It is enough to observe the numerical results as if they were of an ideal magnetic circuit, the magnetic flux of the air gaps under the U-core obtained with the 3D-FEM are not identical. The same happens if the magnetic flux in the legs of the U-core and the rotor yoke are observed. The latter is the reason to pose the reluctance network of Fig. 6 that accurately models the leakage flux, through curved trajectories. In contrast to [26] which rectifies the geometries and only considers straight trajectories. Our leakage flux model, through a reluctance network, allows obtaining a synchronous inductance with a difference of the only 4.05% between the analytical model and the numerical variation with 3D-FEM.

The 3D-FEM output of the electromotive force is also an acceptable value and the output electrical variables of the machine reasonably comply with the design values.

Finally, by the analytical and 3D-FEM results, it can be considered that a methodology that successfully designs the TFPMG of 10 kW in low voltage is obtained, in its lumped parameters, electric and magnetic variables.

REFERENCES

- [1] H. Weh and H. May, "Achievable force densities for permanent magnet excited machines in new configurations," in *Proc. Int. Conf. Elect. Mach.*, vol. 3, 1986, pp. 1107–1111.
- [2] G. Henneberger, "Development of a new transverse flux motor," in *Proc. IEE Colloq. New Topol. Permanent Magnet Mach.*, London, U.K., 1997, pp. 1–6, doi: [10.1049/ic:19970518](https://doi.org/10.1049/ic:19970518).
- [3] A. J. Mitcham, "Transverse flux motors for electric propulsion of ships," in *Proc. IEE Colloq. New Topol. Permanent Magnet Mach.*, London, U.K., 1997, pp. 1–6, doi: [10.1049/ic:19970520](https://doi.org/10.1049/ic:19970520).
- [4] W. M. Arshad, T. Backstrom, and C. Sadarangani, "Analytical design and analysis procedure for a transverse flux machine," in *Proc. IEEE Int. Electr. Mach. Drives Conf.*, Cambridge, MA, USA, Jan. 2001, pp. 115–121, doi: [10.1109/IEMDC.2001.939284](https://doi.org/10.1109/IEMDC.2001.939284).
- [5] D. H. Kang, Y. H. Chun, and H. Weh, "Analysis and optimal design of transverse flux linear motor with PM excitation for railway traction," *IEE Proc.-Electr. Power Appl.*, vol. 150, no. 4, pp. 493–499, Jul. 2003, doi: [10.1049/ip-epa:20030191](https://doi.org/10.1049/ip-epa:20030191).
- [6] M. R. Dubois and H. Polinder, "Study of TFPM machines with toothed rotor applied to direct-drive generators for wind turbines," *Proc. Nordic Workshop Power Ind. Electron.*, Norway, Oslo, 2004, pp. 1–9.
- [7] J. F. Gieras, "Performance characteristics of a transverse flux generator," in *Proc. IEEE Int. Conf. Electr. Mach. Drives*, San Antonio, TX, USA, May 2005, pp. 1293–1299, doi: [10.1109/IEMDC.2005.195889](https://doi.org/10.1109/IEMDC.2005.195889).
- [8] M. R. Dubois, H. Polinder, and J. A. Ferreira, "Comparison of generator topologies for direct-drive wind turbines," in *Proc. NORPIE*, 2000, pp. 22–26.
- [9] D.-J. Bang, H. Polinder, G. Shrestha, and J. A. Ferreira, "Comparative design of radial and transverse flux PM generators for direct-drive wind turbines," in *Proc. 18th Int. Conf. Electr. Mach.*, Vilamoura, Portugal, Sep. 2008, pp. 1–6, doi: [10.1109/ICELMACH.2008.4800027](https://doi.org/10.1109/ICELMACH.2008.4800027).
- [10] D. Bang, H. Polinder, G. Shrestha, and J. A. Ferreira, "Design of a lightweight transverse flux permanent magnet machine for direct-drive wind turbines," in *Proc. IEEE Ind. Appl. Soc. Annu. Meeting*, Edmonton, AB, Canada, Oct. 2008, pp. 1–7, doi: [10.1109/08IAS.2008.71](https://doi.org/10.1109/08IAS.2008.71).
- [11] A. Zavvos, A. S. McDonald, and M. Müller, "Electromagnetic and mechanical optimisation of direct-drive generators for large wind turbines," in *Proc. 5th IET Int. Conf. Power Electron., Mach. Drives (PEMD)*, Brighton, U.K., 2010, pp. 1–6, doi: [10.1049/cp.2010.0066](https://doi.org/10.1049/cp.2010.0066).
- [12] O. Keysan, M. Mueller, A. McDonald, N. Hodgins, and J. Shek, "Designing the c-gen lightweight direct drive generator for wave and tidal energy," *IET Renew. Power Gener.*, vol. 6, no. 3, pp. 161–170, May 2012, doi: [10.1049/iet-rpg.2009.0213](https://doi.org/10.1049/iet-rpg.2009.0213).
- [13] A. Argeseanu, F. T. V. Nica, E. Ritchie, and K. Leban, "A new geometrical construction using rounded surfaces proposed for the transverse flux machine for direct drive wind turbine," in *Proc. Int. Conf. Optim. Electr. Electron. Equip. (OPTIM)*, Bran, Romania, May 2014, pp. 415–420, doi: [10.1109/OPTIM.2014.6850953](https://doi.org/10.1109/OPTIM.2014.6850953).
- [14] J.-H. Oh and B.-I. Kwon, "Design, optimization, and prototyping of a transverse flux-type-switched reluctance generator with an integrated rotor," *IEEE Trans. Energy Convers.*, vol. 31, no. 4, pp. 1521–1529, Dec. 2016, doi: [10.1109/TEC.2016.2562124](https://doi.org/10.1109/TEC.2016.2562124).
- [15] M. A. Patel and S. C. Vora, "Analysis of a fall-back transverse-flux permanent-magnet generator," *IEEE Trans. Magn.*, vol. 53, no. 11, Nov. 2017, Art. no. 8206705, doi: [10.1109/TMAG.2017.2702745](https://doi.org/10.1109/TMAG.2017.2702745).
- [16] M. A. Patel and S. C. Vora, "Analysis of a transverse flux permanent magnet generator with fall-back outer rotor design for wind power generation," *Int. J. Ambient Energy*, vol. 41, no. 11, pp. 1308–1313, Sep. 2020, doi: [10.1080/01430750.2018.1507948](https://doi.org/10.1080/01430750.2018.1507948).
- [17] J. R. Hendershot and T. J. E. Miller, *Design of Brushless Permanent-Magnet Machines*. Venice, FL, USA: Motor Design Books, 2010, p. 178.
- [18] J. Pyrhonen, T. Jokinen and V. Hrabovcova, *Design of Rotating Electrical Machines*. New Delhi, India: Wiley, 2014, p. 614.
- [19] I. Boldea, *Variable Speed Generators*. Boca Raton, FL, USA, CRC Press, 2005, p. 550.
- [20] O. Dobzhanskyi, R. Gouws, and E. Amiri, "On the role of magnetic shunts for increasing performance of transverse flux machines," *IEEE Trans. Magn.*, vol. 53, no. 2, Feb. 2017, Art. no. 8100808, doi: [10.1109/TMAG.2016.2621047](https://doi.org/10.1109/TMAG.2016.2621047).
- [21] *Rotating Electrical Machines—Part 2-1: Standard Methods for Determining Losses and Efficiency From Tests (Excluding Machines for Traction Vehicles)*, document IEC 60034-2-1, 2014.
- [22] S. Figueroa, C. Lehuède, and P. Riquelme, "System for transmitting wave energy absorbed by one or more floating bodies to an energy conversion system located on the coast, and method for transmitting energy," U.S. Patent WO 2020089776 A1, May 7, 2020. [Online]. Available: <https://patentimages.storage.googleapis.com/9b/4e/3b/9f0171f690caaa/WO2020089776A1.pdf>

- [23] D.-J. Bang, H. Polinder, G. Shrestha, and J. A. Ferreira, "Ring-shaped transverse flux PM generator for large direct-drive wind turbines," in *Proc. Int. Conf. Power Electron. Drive Syst. (PEDS)*, Taipei, Taiwan, Nov. 2009, pp. 61–66, doi: [10.1109/PEDS.2009.5385933](https://doi.org/10.1109/PEDS.2009.5385933).
- [24] R. Kumar, Z.-Q. Zhu, A. Duke, A. Thomas, R. Clark, Z. Azar, and Z.-Y. Wu, "A review on transverse flux permanent magnet machines for wind power applications," *IEEE Access*, vol. 8, pp. 216543–216565, 2020, doi: [10.1109/ACCESS.2020.3041217](https://doi.org/10.1109/ACCESS.2020.3041217).
- [25] J. J. Grainger and W. D. Stevenson, *Sistemas Eléctricos de Potencia*. México, North America: McGraw-Hill, 1996, p. 740.
- [26] M. F. J. Kremers, J. J. H. Paulides, and E. A. Lomonova, "Analytical 3-D design of a transverse flux machine with high power factor," in *Proc. Int. Conf. Sustain. Mobility Appl., Renew. Technol. (SMART)*, Kuwait, Kuwait, Nov. 2015, pp. 1–5, doi: [10.1109/SMART.2015.7399243](https://doi.org/10.1109/SMART.2015.7399243).



CRISTHIAN BECKER (Member, IEEE) was born in Santiago, Chile. He received the B.Sc. degree in electrical engineering from the University of Santiago, in 2003, and the M.Sc. degree in electrical engineering from the Federal University of Santa Catarina, Brazil, in 2016, where he is currently pursuing the Ph.D. degree in electrical engineering. He is also an Associate Professor with the Department of Electrical Engineering, University of Santiago of Chile. His research interests include

electric machines, design of permanent magnet generators, and energy efficiency. He is also a member of the International Compumag Society and SBMAG (Brazilian Electromagnetic Society).



MAURICIO VALENCIA FERREIRA DA LUZ was born in Jaguariaíva, State of Parana (PR), Brazil, in 1973. He received the Engineering degree from the State University of Santa Catarina (UDESC), in 1997, and the master's and Ph.D. degrees in the field of energy systems from the Federal University of Santa Catarina (UFSC), in 1999 and 2003, respectively. The subject was related to the studies and development of a method to stray load losses calculation in induction machines. In 1999,

he started his doctorate thesis at UFSC. From April 2001 to October 2002, he studied with the University of Liège, Belgium. Its main issue was the development of a software for 3D electromagnetic field calculation using edge elements, taking into account the movement and the feeding circuit. From 2003 to 2005, he was a Professor with the University Center of Jaraguá do Sul, Santa Catarina, Brazil. In December 2005, he became a Permanent Member with the Department of Electrical and Electronic Engineering, UFSC. He is currently a Regular Reviewer for magazines, journals, and several conferences. He has been also working in some research projects financially supported by the Brazilian Federal Research Councils (FINEP—CNPq) and by private companies. He is also very active on industrial consulting. He is a member of SBMAG (Brazilian Electromagnetic Society).



JEAN VIANEI LEITE was born in Cascavel, State of Parana (PR), Brazil, in 1975. He received the Engineering and Ph.D. degrees in electrical engineering from the Federal University of Santa Catarina, Brazil, in 2000 and 2005, respectively. From 2008 to 2009, he was an Assistant Professor with the Electrical Engineering Department, Federal University of Paraná. Since August 2010, he has been a Professor with the Federal University of Santa Catarina. He teaches courses on electrical

machines and electronic power drives. His research interests include numerical modeling of electromagnetic devices, magnetic materials, and magnetic losses.

• • •